3D Bioprinting of Gradient Scaffolds with Biomimetic Capillaries for Osteochondral Regeneration

Fengxi Liang*

Nanyang Technological University, Singapore

Abstract. Osteochondral defects pose significant clinical challenges owing to the complex hierarchical tissue structure and the limited intrinsic regenerative capacity of cartilage. Existing strategies remain constrained by interfacial stress concentration, insufficient vascularization, or both. This study develops a 3D bioprinting strategy that simultaneously integrates continuous gradient scaffolds with biomimetic capillary networks for osteochondral regeneration. The bioinks were formulated with sodium alginate, methylcellulose, and gellan gum as the hydrogel matrix, with Pluronic F127 serving as a thermosensitive fugitive material for vascular channel fabrication. Mesenchymal stem cells, chondrocytes, and osteoblasts were encapsulated for region-specific bioprinting. The gradient scaffolds exhibited porosity ranging from 82.3 ± 3.7% in cartilage regions to 65.8 ± 4.2% in bone regions, with compressive modulus spanning from 0.8 to 68.5 MPa, closely mimicking native tissue properties. Biomimetic vascular networks achieved 95.6 ± 2.1% channel connectivity, facilitating effective nutrient transport. Cell viability exceeded 87% across all regions, and region-specific gene expression was upregulated by 3.2 to 6.3 folds for chondrogenic and osteogenic markers. Functional biological outcomes were confirmed by extracellular matrix deposition, endothelial cell monolayer formation within vascular channels with 89.3 ± 4.2% positive expression of CD31 and VE-cadherin, and controlled release of angiogenic growth factors that promoted in vitro tube formation. The interfacial shear strength of 4.2 ± 0.6 MPa eliminated stress concentration at the cartilage-bone transition. These findings establish a foundation for bioprinted osteochondral constructs with integrated vascularization, and future work will prioritize in vivo validation in animal defect models.

1 Introduction

Osteochondral defects are where cartilaginous tissue is injured along with the underlying bone tissue. Tissue injuries are a major challenge in orthopedic medicine due to their hierarchical structure and ability to repair [1]. A large percentage of patients requiring arthroscopic procedures present with these tissue injuries. The complications that arise during the repair of these injuries are due to the avascular nature of cartilage tissue and the different repair needs of cartilage and bone tissue [2]. In current times, various surgical interventions show a temporary relief to the injured tissue without completely mimicking the natural biomechanical properties of the tissue, which can lead to long-term complications and the need for additional surgeries. The major drawback of the tissue engineering approach is the insufficient level of vascularization in tissue-engineered constructs [3]. The tissue constructs are unable to survive due to the lack of a vascular system for the provision of nutrients and the removal of waste products. This results in a low survival rate for the tissue-integrated cells [4].

The natural osteochondral unit has a gradient architecture that consists of different zones. It has a continuous composition and mechanical properties that range from the hydrated cartilaginous surface tissue to the mineralized bone tissue underneath [5]. Such a complex architecture calls for biomimetic methods that are capable of replicating a gradient at both the macro and micro levels. The latest studies have shown that gradient scaffolds are capable of resulting in better cell differentiation compared to uniform scaffolds [6]. On the other hand, 3D bioprinting has been recognized as a revolutionary method for creating complex tissue structures that has the ability to control the spatial distribution of biomaterials, cells, and biofactors in a predetermined three-dimensional manner [7]. However, existing 3D bioprinting strategies for osteochondral regeneration can be broadly categorized into three types, each with distinct limitations. Monophasic scaffolds with uniform composition fail to satisfy the differential mechanical and biological requirements of cartilage and bone simultaneously. Biphasic scaffolds that separate cartilage and bone layers improve regional specificity but introduce abrupt interfaces prone to stress concentration and delamination under physiological loading. Gradient scaffold designs have partially addressed the interface issue by creating compositional or mechanical transitions, yet most studies focus on a single gradient dimension without incorporating vascularization. The absence of an integrated vascular network remains a critical barrier for nutrient delivery

* Corresponding author: liangfengxi2027@163.com

and waste removal in large-volume tissue-engineered constructs, directly limiting cell survival and tissue maturation.

To address these limitations, the present study develops a 3D bioprinting strategy that simultaneously integrates continuous gradient scaffolds with biomimetic capillary networks for osteochondral regeneration. This strategy differs from existing approaches in three specific aspects. First, the scaffold employs a continuous gradient in porosity, composition, and mechanical properties from the cartilage surface to the subchondral bone, rather than discrete layering, which eliminates abrupt interfaces and reduces stress concentration at the transition zone. Second, a biomimetic capillary network is embedded within the gradient scaffold during the printing process, directly addressing the vascularization deficiency that limits nutrient transport in conventional gradient designs. Third, a multi-material collaborative bioprinting workflow constructs gradient structures and vascular channels in a single fabrication process, avoiding the need for separate post-processing steps to introduce vascular channels. The objective of this study is to fabricate and characterize these integrated scaffolds and to evaluate their structural, mechanical, and biological performance in vitro.

2 Materials and methods

2.1 Biomimetic gradient scaffold design

In natural osteochondral tissues, specific gradient characteristics can be observed in different zones. When histological tests are carried out on these tissues, four main zones can be identified. The zones include superficial cartilage (5-15% collagen type II), middle zone (10-20% proteoglycans), deep zone (25-35% collagen type X), and calcified subchondral bone (40-60% hydroxyapatite). The design of the scaffold is intended to mimic these characteristics using computer modeling.

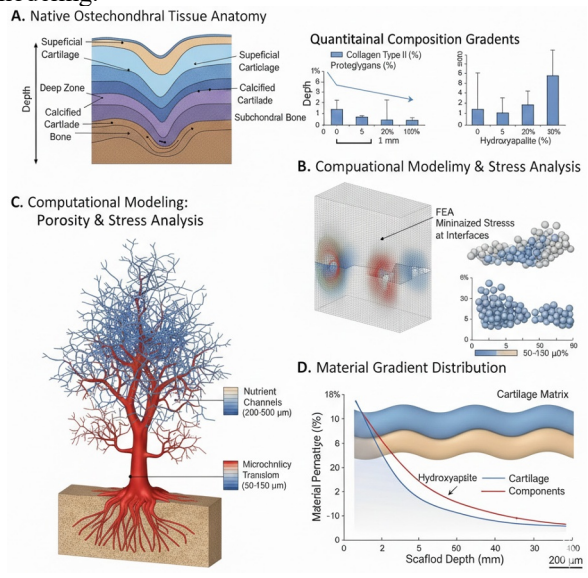

Fig. 1. Biomimetic Gradient Scaffold Design Scheme.

Optimal porosity gradients were determined. The porosity gradients range from 80 to 90% for the cartilage region and 60 to 70% for the bone region. The design minimizes stress concentrations on the tissue interface. The capillary network design is based on physiological patterns of blood vessel formation. The nutrient vessel with a diameter range of 200 to 500 µm is found in the bone layer. The microchannels with a diameter range of 50 to 150 µm are found in the cartilage matrix, as depicted in Fig. 1. The material gradients use gradients instead of layering to ensure tissue integration without weakness on the interface.

2.2 Bioink formulation and cell encapsulation

In addition, the bioink system used a combination of natural and synthetic polymers for optimal performance. The hydrogel system used was composed of sodium alginate (2–4% w/v), methyl cellulose (1–2% w/v), and gellan gum (0.5–1% w/v). The hydrogel system was used for the shear-thinning properties required for the extrusion-based printing technique. The rheological tests indicated a range of 800–2000 Pa·s at the resting state, as well as 50–200 Pa·s during the printing process.

The cell encapsulation methods ensured that the cell viability remained high throughout the entire cell bioprinting procedure. The mesenchymal stem cell culture and chondrocytes were embedded into cartilage-targeting bioinks at a cell density of 1.5 to 2.5 x 106 cell/mL. On the other hand, the osteoblasts were embedded into bone-targeting bioinks at similar cell densities. The osmotic stabilizers and anti-apoptotic agents ensured the cell viability remained at least 85% throughout the cell bioprinting procedure. The cross-linking mechanism used involved ionic gelation using calcium chloride solution (50-100 mM) for instantaneous cross-linking. UV irradiation was applied as a secondary cross-linking step to enhance the long-term stability of the hydrogel network, complementing the ionic gelation to achieve the desired degradation profile.

2.3 3D bioprinting process and fabrication

The bio-printing system employed a multi-material extrusion bio-printing technique with the ability to control various parameters of operation. The system employed pneumatic dispensers for controlling pressure levels (0.1 to 10 bar) and temperature levels (4 to 37°C), depending on the bioink materials used for bio-printing. The speed of bio-printing was optimized for cartilage bioinks (8 to 15 mm/s) and bone bioinks (5 to 10 mm/s), depending on flow modeling analysis.

In addition, the nozzle configuration involved standard conical tip geometries for structural printing, with a diameter of 200-400 µm, as well as coaxial needles for vascular channels. The coaxial needle configuration had an inner diameter of 150 µm and an outer diameter of 300 µm, as shown in Fig. 2. The capillary network fabrication involved direct extrusion of Pluronic F127 (Poloxamer 407) as a thermosensitive

fugitive material, followed by cell-containing bioink encapsulation. After printing, the constructs were cooled to 4°C to liquefy and remove the Pluronic F127, forming hollow vascular channels. The layer height was set at 150-250 µm, which ensured interlocking while reducing printing time for cell viability.

The post-processing included a particular sequence of cross-linking processes. The processes included immediate ionic gelation, which was carried out to ensure that geometries were preserved. This was followed by ultraviolet light, which was used at a wavelength of 365 nm and a power density of 10-15 mW/cm² for 3-5 minutes to attain final properties. The maturation of scaffolds was carried out in perfusion bioreactors at a rate of 0.1-0.5 mL/min over a period of 2-4 weeks.

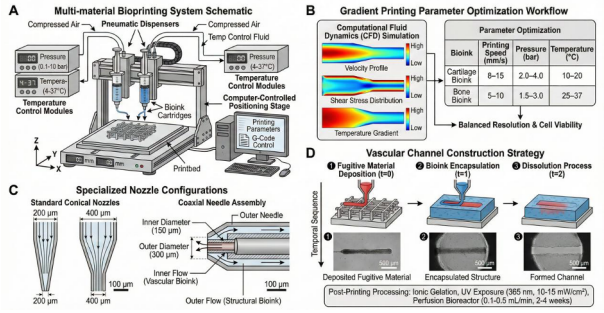

Fig. 2. 3D Bioprinting Process and Parameters.

2.4 Characterization and biological evaluation

In the characterization of scaffolds, various techniques were utilized in a complementary manner for the assessment of structural as well as biological properties. µCT scans with a resolution of 10 µm were performed for the assessment of porosity distribution as well as the interconnectivity of different regions of the scaffolds. Scanning electron microscopy was utilized for the assessment of surface morphology, whereas energy dispersive X-ray spectroscopy was performed for the assessment of the distribution of minerals in the scaffolds.

For the evaluation of the vascular network, perfusion studies using fluorescent microspheres of 1 to 10 microns were carried out. The patency of the channels was evaluated by this technique on the biomimetic capillary network. The mechanical properties were evaluated by nanoindentation on a 100-micron resolution scale over the elastic modulus range of cartilage (0.1 to 1 MPa) to bone tissue (10 to 100 MPa).

For biological evaluation, scaffolds were seeded with fluorescently labeled cell populations. Cell behavioral monitoring was performed for cell proliferation, differentiation, and matrix deposition over 28 days. The biological evaluation was performed using well-characterized biochemistry assays. Cell quantification was performed by measuring DNA content; differentiation into an osteogenic lineage was measured by alkaline phosphatase activity, while deposition of a cartilaginous matrix was measured by glycosaminoglycan content. A one-way ANOVA test with Tukey's analysis was performed for a quantitative analysis of all the conditions ($n > 6$, $p < 0.05$).

3 Results

3.1 Gradient scaffold architecture and capillary networks

The multi-material collaborative 3D bioprinting technique was successfully used for the creation of biomimetic scaffold structures that presented gradient properties. Moreover, the analysis for porosity was performed for the scaffolds using the micro-CT method. This analysis showed that it was possible to create scaffolds that presented both vertical porosity and pore size gradient properties. In this regard, cartilage was shown to present a porosity of 82.3 ± 3.7% with pore size ranging from 150-300 µm, while the bone presented a porosity of 65.8 ± 4.2% with a pore size ranging from 300-600 µm. The analysis for the structural fidelity of the scaffolds showed that scaffolds presented a printing accuracy of ±15 µm, while bonding strength was shown to be 2.8 ± 0.4 MPa.

The microchannel structures of 50-150 µm were presented in cartilage regions of the biomimetic capillary structures, whereas main channel structures of 200-500 µm were presented in bone regions, where channel connectivity was found to be 95.6 ± 2.1%. As depicted in Fig. 3, the scaffolds were capable of showing a continuous transition between cartilage and bone tissue, along with pore architecture showing unique directional gradient distribution. Surface roughness/morphology, as studied by scanning electron microscopy, has been found to change in a similar manner in different areas as compared to the native tissue. The scaffolds with pore diameters ranging from 90 to 120 µm were found to be conducive for cartilage formation for MSCs, whereas scaffolds with pore diameters of 300 µm were found to be conducive for osteogenesis. The gradient interface did not show any signs of delamination and hence facilitated a smooth transition to an optimal 3D microenvironment.

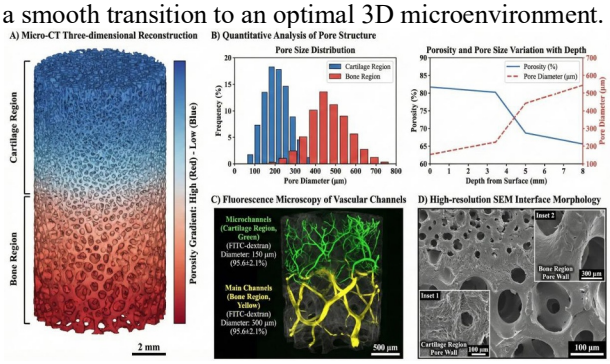

Fig. 3. Gradient Scaffold Architecture and Capillary Networks.

3.2 Mechanical properties and gradient distribution

The mechanical properties of the gradient scaffolds were observed to be in the range of the mechanical properties of the native tissues. The results obtained from the

compressive modulus tests showed that the modulus of the cartilage region was 0.8 0.2 MPa, for the transition region it was 15.6 3.4 MPa, and for the bone region it was 68.5 8.7 MPa. On the other hand, the data from uniaxial compression tests showed that porosity (φ) was inversely related to the compressive modulus (E) and the yield stress (y) and the relationships were given by E (1-φ) ^1.27 and y (1-φ) ^1.37.

The results for the interface bonding strength evaluation indicated that the shear strength was 4.2 ± 0.6 MPa at the cartilage-bone transition regions. There were no delamination failure phenomena. The results for the permeability evaluation indicated that the permeability in the cartilage region and bone region was 2.3 × 10^-14 m² and 8.7 × 10^-15 m², respectively. The permeability results were consistent with the requirements for nutrient supply. As shown in Table 1, the overall performance indicators for the scaffolds were in the physiological ranges, and the gradients in the mechanical properties were strong.

Table 1. Comprehensive Performance Analysis of Gradient Scaffolds.

Parameters	Cartilage Region	Transition Zone	Bone Region	Native Tissue
Compressive Modulus (MPa)	0.8±0.2	15.6±3.4	68.5±8.7	0.2-320
Porosity (%)	82.3±3.7	74.2±4.1	65.8±4.2	70-85
Pore Size (μm)	150-300	250-400	300-600	100-500
Permeability (×10^-14 m²)	2.3±0.4	1.8±0.3	0.87±0.2	0.5-3.0
Interface Strength (MPa)	-	4.2±0.6	-	3-6

3.3 Cellular response and osteochondral differentiation

Both cell viability and differentiation had region-specific patterns of performance. The results from the MTT assay indicated that the cell survival rate was 91.4 ± 2.8% in the cartilage regions, whereas the cell survival rate was 87.6 ± 3.2% in the bone regions. The results from the Live/Dead fluorescence staining indicated that the cells had adhered well to the gradient scaffolds. The results from the quantitative PCR analysis indicated that the expression of Sox9 was 3.2 times higher, whereas the expression of Col2a1 was 4.8 times higher in the cartilage regions. The expression of Runx2 was 5.7 times higher, whereas the expression of Col1a1 was 6.3 times higher in the bone regions.

Sox9 is a significant factor for chondrogenic differentiation. Sox9 is recognized as an early marker for the formation of chondrocytes. Immunofluorescence staining confirmed that the expression of type II collagen had been significant in the cartilage region. The expression of type I collagen and osteocalcin had been significant in the bone region. As depicted in Figure 4, the cells show phenotypic characteristics. The morphology of the chondrocytes was observed to be spherical in shape and to produce a large amount of proteoglycan-rich matrix. The morphology of the osteoblasts was observed to be polygonal in shape and to produce matrix mineral deposits. The content of glycosaminoglycan was observed to be 28.6 ± 4.3 μg/mg in the cartilage regions and the activity of alkaline phosphatase was observed to be 15.2 ± 2.7 U/mg protein in the bone regions by ELISA. The results were further strengthened by the results obtained from the Western blot.

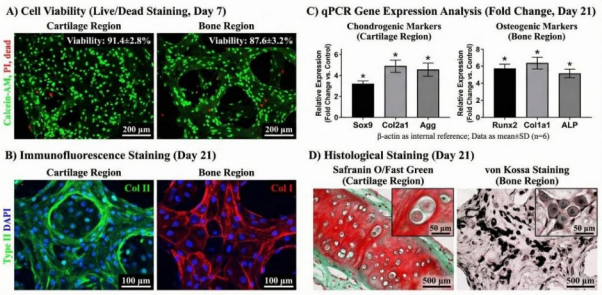

Fig. 4. Cellular Response and Osteochondral Differentiation.

3.4 Biomimetic vascularization and integration

The biomimetic capillary networks exhibited excellent functionalization properties and tissue integration capabilities during in vitro culture. The vascular channels exhibited satisfactory performance for the transportation of nutrients based on the results of the fluorescent microsphere perfusion assays, where 1 μm fluorescent microspheres exhibited 94.2 ± 3.5% and 10 μm microspheres exhibited 78.6 ± 5.1%. When we seeded the channels with HUVECs, the cells adhered and spread effectively across the inner surfaces. By day 14, this resulted in a continuous endothelial monolayer with high expression levels (89.3 ± 4.2%) for both CD31 and VE-cadherin.

The scaffold managed to release VEGF (85.6 6.8%) and bFGF (79.3 5.4%) at a constant pace through the critical 7-to-14-day period, in line with growth factor kinetics. Moreover, the in vitro angiogenesis assays supported this bioactivity, as the conditioned medium induced a marked increase in tube formation, mainly a 2.8-fold rise in length and 3.4-fold jump in branch points. Lastly, the cartilage-bone interface was free of fibrous tissue indicating enhanced integration and increased bonding strength. The results obtained from immunohistochemical staining indicated that integrin beta 1 and fibronectin were upregulated in the interface region, thereby increasing the interaction between the cells and the matrix.

The results obtained from the quantitative PCR analysis indicated that the expression of angiogenesis-related genes such as VEGF, Ang-1 and Tie-2 was increased in the vascularized region. The biomimetic capillary network is thus provided with all the essential functional characteristics for tissue regeneration.

4 Discussion

The successful fabrication of scaffolds with 3D bio-printed gradient distribution is reported in this

research work. The biomimetic capillary gradient distribution has been found to be very effective. The porosity of scaffolds has been found to vary smoothly from 82.3 ± 3.7% for cartilage regions to 65.8 ± 4.2% for bone regions. At the same time, the compressive modulus has been found to vary smoothly from 0.8 MPa to 68.5 MPa. The gradient architecture of scaffolds has been found to create region-specific microenvironments that are favorable for directional differentiation. The chondrogenic differentiation is stimulated, according to the research, as seen with the increase of Sox9 and Col2a1 genes by 3.2-fold and 4.8-fold, respectively. Likewise, osteogenic differentiation is shown to be stimulated with an increase in the expression of Runx2 and Col1a1 genes by 5.7-fold and 6.3-fold, respectively. A comparison with representative existing strategies clarifies the specific contributions of the present approach. Kilian et al. (2020) fabricated multi-layered mineralized constructs with distinct cartilage and bone phases, yet the discrete layer boundaries created mechanical discontinuities at the interface. In contrast, the continuous porosity gradient (82.3% to 65.8%) and modulus gradient (0.8 to 68.5 MPa) achieved in this study provide a smooth mechanical transition that falls within the native tissue range (Table 1). Sun et al. (2020) demonstrated dual-factor releasing gradient constructs that promoted anisotropic cartilage regeneration, but their design did not incorporate a vascular network for nutrient delivery. The present study addresses this gap by integrating capillary channels with 95.6 ± 2.1% connectivity, enabling effective perfusion as confirmed by fluorescent microsphere assays (94.2% passage rate for 1 μm microspheres). Chae et al. (2023) advanced vascularized bioprinting strategies, though their work focused on vascularization as an independent objective rather than combining it with gradient scaffold architecture. The simultaneous integration of both gradient structure and vascular network in a single printing workflow represents the principal technical distinction of the current study.

The design of the vascular network facilitated tissue integration. The channel connectivity of 95.6±2.1% enabled effective nutrient transportation. The release of VEGF and bFGF promoted endothelialization [8]. The gradient scaffolds outperformed the monophasic and biphasic scaffolds by reducing interfacial stress concentration. The interfacial shear strength was 4.2±0.6 MPa, showing an enhanced long-term stability [9].

Based on the analysis of the mechanisms of the osteochondral regeneration technology, it can be noted that the gradients are essential for the spatial organization of the differentiation processes of chondrocytes to osteoblasts. This is achieved through the control of the secretion of the extracellular matrix. However, the technology is associated with some challenges such as the resolution of the printing processes and the biocompatibility of the technology [10]. The future prospects of the technology are improved by the resolution of the printing processes. Despite the prospects of the technology, some challenges are evident. The challenges are associated with the production process of the technology to treat osteochondral defects. It should be noted that the current study is based on in vitro characterization and biological evaluation. Although the functional biological outcomes, including region-specific differentiation, extracellular matrix deposition, and vascular channel endothelialization, provide supportive evidence for the regenerative potential of the gradient scaffolds, in vivo validation in animal osteochondral defect models is necessary to confirm long-term tissue regeneration and functional recovery.

5 Conclusion

The study is an advancement in osteochondral tissue engineering by incorporating gradient scaffolding structures and biomimetic capillary networks using the latest technology in 3D bioprinting. The study indicated that collaborative multi-material bioprinting can create scaffolding structures that have inherent porosity gradients (82.3 ± 3.7% to 65.8 ± 4.2%) and mechanical property gradients (0.8-68.5 MPa) similar to native osteochondral tissues. The integration of biomimetic capillary networks that have 95.6 ± 2.1% connectivity is a milestone in addressing the vascularization challenge in tissue engineering.

Significant evidence for region-specific cellular differentiation in gradient microenvironments is provided by this study, indicated by a 3.2- to 6.3-fold upregulation of chondrogenic and osteogenic marker genes. The bonding strength between the interfaces is 4.2 ± 0.6 MPa, which overcomes the problem of stress concentration. This provides a superior method for ensuring long-term stability compared to traditional methods. This study has significant clinical importance for the therapeutic management of complex osteochondral defects, which are still not optimally addressed.

The advancement in the integration of structural gradients along with vascularization is a new kind of advancement that goes far beyond the application in orthopedics. This technology platform provides the fundamental principles for the development of the next generation of bio-printed tissues that possess better integration capabilities. The achievement of tissue regeneration is a highly viable concept for redefining the present treatment paradigms in the realm of reconstructive medicine. Future work will focus on in vivo validation of the gradient scaffolds in animal osteochondral defect models to evaluate their long-term regenerative efficacy and clinical translational potential.

References

1. Wang, Q., Zhu, W., Wang, R., & Weng, X. (2025). Hierarchical 3D-printed scaffolds for osteochondral regeneration: From biomimetic design to functional integration. International Journal of Bioprinting, 11(4), 4-31.
2. Du, J., Zhu, Z., Liu, J., Bao, X., Wang, Q., Shi, C., ... & Li, D. (2023). 3D-printed gradient scaffolds for osteochondral defects: Current status and

perspectives. International Journal of Bioprinting, 9(4), 724.

3. Chae, S., Ha, D. H., & Lee, H. (2023). 3D bioprinting strategy for engineering vascularized tissue models. International Journal of Bioprinting, 9(5), 748.
4. Shiwarski, D. J., Hudson, A. R., Tashman, J. W., Bakirci, E., Moss, S., Coffin, B. D., & Feinberg, A. W. (2025). 3D bioprinting of collagen-based high-resolution internally perfusable scaffolds for engineering fully biologic tissue systems. Science Advances, 11(17), eadu5905.
5. Corrado, F., Di Maio, L., Palmero, P., Coppola, B., Abbas, Z., La Gatta, A., ... & Scarfato, P. (2025). Vat photo-polymerization 3D printing of gradient scaffolds for osteochondral tissue regeneration. Acta Biomaterialia.
6. Sun, Y., You, Y., Jiang, W., Wang, B., Wu, Q., & Dai, K. (2020). 3D bioprinting dual-factor releasing and gradient-structured constructs ready to implant for anisotropic cartilage regeneration. Science Advances, 6(37), eaay1422.
7. Kilian, D., Ahlfeld, T., Akkineni, A. R., Bernhardt, A., Gelinsky, M., & Lode, A. (2020). 3D Bioprinting of osteochondral tissue substitutes–in vitro-chondrogenesis in multi-layered mineralized constructs. Scientific Reports, 10(1), 8277.
8. Zhu, W., Qu, X., Zhu, J., Ma, X., Patel, S., Liu, J., ... & Chen, S. (2017). Direct 3D bioprinting of prevascularized tissue constructs with complex microarchitecture. Biomaterials, 124, 106-115.
9. Elango, J., & Zamora-Ledezma, C. (2025). Rheological, structural, and biological trade-offs in bioink design for 3d bioprinting. Gels, 11(8), 659.
10. Paradiso, A., Volpi, M., Martinez, D. C., Jaroszewicz, J., Costantini, M., & Swieszkowski, W. (2024). Engineering Biomimetic Microvascular Capillary Networks in Hydrogel Fibrous Scaffolds via Microfluidics-Assisted Co-Axial Wet-Spinning. ACS Applied Materials & Interfaces, 16(48), 65927-65941.